Journal of Analytical and Applied Pyrolysis 192 (2025) 107342

Contents lists available at ScienceDirect

Journal of Analytical and Applied Pyrolysis

journal homepage: www.elsevier.com/locate/jaap

Controlled hydrothermal carbonization of wood-derived lignin-rich lignocellulose: Redefining pyrolytic pathways to tailored biochar and hydrogen-enriched syngas

Muhammad Rizwan [a], Asma Leghari [b], Akash Kumar [c], Azhar Laghari [d], Adil Mansoor [e], Muhammad Asif Nawaz [f,*], Xiaolong Zhou [a,*]

[a] International Joint Research Center for Green Energy and Chemical Industry, School of Chemical Engineering & Technology, East China University of Science & Technology, Shanghai 200237, China
[b] Institute of Clean Coal Technology, East China University of Science and Technology, Shanghai 200237, China
[c] School of Civil Engineering, Guangzhou University, Guangzhou 510006, China
[d] College resources Environment Shanxi Agriculture University, Shanxi 030801, China
[e] College of Physics and Optoelectronic Engineering, Shenzhen University, Shenzhen 518060, China
[f] Department of Inorganic Chemistry and Material Sciences Institute of Seville, University of Seville-CSIC, Seville 41092, Spain

ARTICLE INFO

Keywords:
Lignin-rich lignocellulosic biomass
Hydrothermal carbonization
Pyrolysis
Syngas
Biochar
Tar composition
Biomass valorization

ABSTRACT

This research illustrates the efficacy of hydrothermal carbonization (HTC) as a pretreatment method to improve the pyrolytic performance of wood-derived lignin-rich lignocellulosic biomass (LB), supported by thorough characterization of its derived products such as syngas, tar, and biochar. A systematic comparison of non-HTC-treated LB and HTC-treated LB through their respective pyrolytic-derived biochar (NLB, HLB) obtained across temperatures (400-1000°C) revealed their basic structural and reactivity variations. HTC resulted in a new carbonyl peak with a 28 % increase in C═O concentration in derived biochar, with partial aromatization evidenced by C═C bonds at 1509 cm^{-1} . Spectroscopic analysis confirmed that HTC promoted a defective carbon structure in derived biochar while enhancing its crystallinity and maintaining its integrity even at higher temperatures. XPS analysis demonstrated that at 1000°C, HLB-T_{10} retained active oxygen functionalities, while its associated pyrolytic products H_2 and CO boosted from 22.45 % to 40.4 % and 32.3–33.4 %, respectively, with drastically lowered CO_2 emissions from 39.95 % to 11.5 %. Regulated deoxygenation routes cause tar composition to shift toward desirable aromatic chemicals. This comprehensive strategy offers a sustainable valorization technique that increases syngas generation efficiency, lowers emissions, and optimizes biorefinery product selection.

1. Introduction

The growing global dedication towards sustainable resource management and the development of circular bioeconomy has intensified scientific interest in converting biomass-derived materials into high-value bioenergy products via alternative valorization technologies [1]. Among the various thermochemical strategies, pyrolysis [2,3] stands out as a prominent pathway for transforming biomass into biochar [4], syngas [5], and tar [6] (including phenols, ethers, polycyclic aromatic hydrocarbons, and other organic substances) [7], thereby having the potential to replace traditional fuels. The biomass combustion process optimizes its conversion into valuable energy products, boasting an impressive fuel energy conversion rate of up to 95.5–99.5 % [8]. Meanwhile, second-generation biofuels can also be produced from aquatic plants, grass, forestry, municipal, agricultural waste[9], and industrial waste lignocellulosic biomass [10]. Lignocellulosic biomass (LCB) [11], a renewable, carbon-rich resource composed primarily of cellulose, hemicellulose, and lignin [12], offers immense potential for such valorization strategies due to its abundance and structural complexity [13]. Lignin, which constitutes approximately 15–30 % of LCB, is a highly cross-linked, aromatic biopolymer that provides structural rigidity to plant cell walls [14]. Despite its abundance, its efficient utilization remains limited due to its heterogeneous chemical structure [15], complex inter-unit linkages [16] (β-O-4, C-C, C-O), and high

* Corresponding authors.
E-mail addresses: mnawaz@us.es (M.A. Nawaz), xiaolong@ecust.edu.cn (X. Zhou).

https://doi.org/10.1016/j.jaap.2025.107342
Received 23 May 2025; Received in revised form 10 August 2025; Accepted 20 August 2025
Available online 21 August 2025

oxygen content [17], which complicate its depolymerization and conversion into value-added products [18], resulting in 40 % being burned for energy utilization in the pulping process [19]. Given its complicated structure, advanced techniques such as biological and thermochemical processes are required to decompose lignin's rich LCB resilient aromatic framework while preserving product distribution and selectivity [20, 21]. Conventional processes for LB valorization have mainly focused on various thermochemical conversion techniques, including hydrothermal liquefication, pyrolysis, and gasification [22], thereby necessitating pretreatment strategies to improve product selectivity. However, the ineffective use of LB poses a considerable challenge while simultaneously presenting an opportunity within the framework of biorefinery advancement and sustainable production of chemicals. Because of these challenges associated with traditional processing, scientists are investigating more creative yet effective LB valorization techniques.

Over the past few decades, there has been an increasing interest in HTC as an effective pretreatment technique for biomass processing. HTC induces substantial structural modifications in biomass distinctively under subcritical water conditions (180–260°C, 2–6 MPa) [23] by undergoing through hydrolysis, dehydration, decarboxylation, and condensation reactions. Dehydration (loss of H_2O) and decarboxylation (loss of CO_2) are dominant pathways, effectively removing oxygen from the solid and yielding a hydrophobic, carbon-rich HC [24]. Although, HTC effectively transforms biomass into energy-dense HC, however, 30–50 % of biomass carbon may dissolve in the process water (PW), which contains oxygenated compounds (e.g., acetic and formic acids, furfural, phenolics) and poses disposal challenges due to high COD and toxicity [25]. Recent study [24] proposes that PW recirculation improves HC yield (~10.5 wt% at 180 °C; ~18 wt% over five cycles) by enriching reactive intermediates, enhancing dehydration and decarboxylation. Following the same trend, synergistic interaction between OPM and PW also facilitated to increase HC mass yield to 11 wt% along with increased carbon and energy yield by 26.1 % and 27.1 % respectively [26]. Alternatively, anaerobic digestion can valorize PW organics into biogas, though phenolic inhibitors require careful management [25].

Upon application to LB, HTC treatment causes its depolymerization [27], condensation or polymerization [28], ether bond cleavage [29], molecular weight reduction [30], and changes in functional group distribution [31], making it more thermally stable and enabling better valorization. Hemicellulose and cellulose components hydrolyze into soluble sugars and oligomers, which further dehydrate to furan compounds and organic acids, while lignin fragments undergo repolymerization into carbon-rich HC [25]. These structural modifications are essential for increasing the thermal resilience of biomass and enhancing its reactivity under subsequent pyrolytic conditions. Unlike conventional pyrolysis, which requires pre-drying of biomass, HTC effectively processes moist substrates and produces a hydrochar (HC) with a high carbon content and reformed oxygen functionality, making it a suitable intermediate for gas and liquid phase valorization.

Integrating HTC with pyrolysis represents exciting advancements for biomass valorization [32], thereby enhancing product yields, selectivity, and energy efficiency compared to single-process pyrolysis methods [33]. Moreover, the aqueous features of HTC enable it to be especially appropriate for the treatment of moisture-enriched LCB [34], thereby reducing the energy-demanding drying processes typically necessary before conventional pyrolysis. The pyrolysis of HTC-treated microalgal biomass exhibits markedly different reaction pathways than untreated biomass, primarily owing to the structural alterations induced during hydrothermal treatment [32]. These modifications may encompass selective cleavage linkages (β-O-4, α-O-4, and 5–5′) followed by changes in functional group distribution, and facilitating lignin conversion to valuable products [35]. Recent advancements in analytical methodologies have facilitated a more comprehensive characterization of the intermediate products generated during HTC treatment and the final products acquired post-pyrolysis. Advanced thermal analysis techniques, GC-MS, and 2D GC, FTIR are all employed to uncover complex reaction pathways and the relationships between process variables and product distributions [36]. Such insights are crucial for formulating predictive models and optimizing process parameters for desired product objectives. Thus, the integrated HTC-Py process for lignin may potentially deliver various energy-intensive valuable products such as phenolic compounds [37], aromatic hydrocarbons [38], and carbon-based materials [39]. The capacity to selectively generate particular compounds or material characteristics by precisely regulating process conditions constitutes a notable benefit of the integrated approach. The process can be customized for various lignin-rich feedstocks, such as kraft lignin, organosolv lignin, and lignosulfonates, each necessitating distinct optimization approaches. Environmental factors are essential in the advancement of these integrated processes. The HTC-Py combination presents numerous ecological benefits, such as diminished energy usage, decreased greenhouse gas emissions relative to traditional thermal processing, and the possibility of water reclamation within the process. Nonetheless, the prospect of enhanced product selectivity and yield, along with the capacity to process wet feedstocks, may offer economic benefits compared to traditional single-process methods. The advancement of effective heat integration strategies and the optimization of process parameters can further improve the financial viability of these systems. Nonetheless, the intricate and stubborn nature of raw LB frequently leads to diminished gas yields, increased tar production, and suboptimal conversion efficiency, thereby constraining its practical uses. HTC is being recognized as a promising approach to alter the structure of LB and improve its performance during pyrolysis. The fundamental processes by which HTC pretreatment enhances LB pyrolysis, specifically regarding gaseous composition, tar reduction, and morphological alterations, are still not well known, despite its potential.

This investigation tackles these deficiencies by methodically examining the pyrolysis characteristics of both commercially available LB and HTC-treated LB through sophisticated analytical approaches to reveal the significant impacts during HTC pretreatment and enhance LB valorization. This study further examines the integration of HTC and pyrolysis for LB valorization, focusing on (I) physicochemical characteristics of NLB and HLB (II) to evaluate the pyrolysis performance for gaseous and bio-oil composition, and (III) insights into the mechanisms of thermal decomposition and the impact of structural modifications on product distribution along with practical implications of HTC pretreatment for LB transformation. This study also provides critical insights into optimizing LB conversion to sustainable bioenergy products by systematically examining the impact of HTC pretreatment on the pyrolysis behavior of derived HC.

2. Materials and methods

2.1. Materials

The feedstock represents a commercially available wood-derived LB material that was obtained from Jiangsu Wecnchang New Material Technology Co., Ltd., and its specific properties are shown in Table 1. This material comprises approximately 89.1 % fiber content and was chosen as a model substrate because of its uniform lignocellulosic structure, which enhances process reproducibility and offers insights into the behavior of LB during pyrolysis. The selected LB material

Table 1
Properties of LB.

Properties	Measured
Ash content (%)	15.5
pH	7.20
Wood fiber content (%)	89.1
Moisture content (%)	4.40
Density (g/cm^3)	1.30

functions as a controlled prototype for analyzing pyrolytic behavior, eliminating the variability associated with lignin wastes. Isopropanol was purchased from Shanghai Boer Chemical Reagent Co., Ltd.

2.2. Hydrothermal carbonization

HTC experiments were conducted in a high-pressure batch reactor (HT-250 J0, HTLAB, Beijing, China). Fig. 1 demonstrates the reactor equipped with a rotating stirrer and PID control system, featuring a maximum operating temperature of 350 °C and a maximum pressure of 30 MPa.

For each experiment, 50 g of dried LB was mixed with 50 mL of deionized water (LB-to-solvent ratio of 1:1, w/v) and heated at 200 °C for 60 min in a sealed reactor. These reaction conditions were selected based on our prior study [40], which showed improved basic fuel properties of the HC. Ar gas was purged through the reaction chamber to remove oxygen and undesired impurities. Following the successful completion of the carbonization reaction, the reactor was cooled, and the HC was collected. Vacuum filtration was employed to separate the HC from the process water. The sample acquired from HTC was dried in an electric oven at 105 °C for 24 h, followed by its careful storage for subsequent characterization. To ensure the reliability of the resultant product, all sets of experiments were performed in duplicate.

2.3. Pyrolysis

The pyrolysis reactor consists of a horizontally placed quartz tube with dimensions 200 mm x 50 mm x 25 mm (length x width x height) as demonstrated in Fig. 1. A temperature controller was coupled to an electrical thermostat using an insulated K-type thermocouple to control the reactor's temperature. During the pyrolysis reaction, a fixed mass of 5 g of LB or HC was placed in a crucible and positioned in the center of the quartz tube. After tightening the reactor's seals, it was purged with N_2 gas at a rate of 600 mL/min, along with the heating rate adjustment at 10 ℃/min. Upon achieving the targeted temperatures at 400 °C, 600 °C, 800 °C, and 1000 °C, the reaction was completed in 30 min. The experiments were conducted twice to ensure consistency and reliability.

2.4. Analytical techniques

The resultant biochar structure was analyzed using FE-SEM, or scanning electron microscopy (ZEISS, Gemini SEM 30). A Micromeritics ASAP-2460 equipment was used to fig. out pore structure and surface area using N_2 adsorption-desorption isotherms at 77 K. A Fourier transform infrared spectrometer (FTIR, Thermo Fisher Scientific, USA) was used to examine the functional groups in the derived biochar samples. Using a LabRAM HR800-LS55 spectrometer (Horiba Jobin Yvon, France) fitted with a silicon-based CCD detector and optical microscope, the Raman analysis was performed at ambient temperature. To avoid thermal damage to the sample, a 532 nm Nd-YAG laser at 5 mW power was used, focusing on the 1800–1000 cm^{-1} range, which offered adequate structural information. Acquisition parameters featured 0.65 cm^{-1} spectral resolution over 20 sec scans. Using XRD patterns from an Ultima IV diffractometer (Japan), crystallographic phase determination was carried out. While C 1 s spectra were examined by using the ESCALAB 250Xi XPS system (USA) with an Al K\u03b1 X-ray source (1486.6 eV), operated at 20 eV pass energy, 0.05 eV energy steps. The gas composition (H_2, CH_4, C_2H_6, C_2H_4, CO, CO_2) was analyzed using a gas chromatograph (GC 990 A) with two columns (5 A and GDX-104) and a thermal conductivity detector (TCD), with Ar acting as the carrier medium. Isopropanol was used as a solvent to extract tar from the distillation tubes, which comprised a condensed phase of tar. The composition and relative content of the liquid products were analyzed with the aid of a Gas Chromatography-Mass Spectrometer (GC/MS, Agilent 7980 A/5975 C) equipped with an Agilent HP-5MS capillary column (30 m x 0.25 mm×0.25 μm). The GC was initially held at 50 °C for 5 min, then heated to 280°C with a heating rate of 8 °C/min and held for 5 min.

3. Results and discussion

3.1. Ultimate and proximate analysis of derived biochar

The ultimate analysis indicated that HTC pretreatment of LB substantially alters its thermal degradation pathway. With the increase in pyrolysis temperature, NLB biochar grows progressively with carbon content, whereas HLB demonstrates a declining carbon trend due to enhanced syngas synthesis, as evidenced in Section 3.5. This signifies a transition in product selectivity from solid biochar to gaseous fractions, consistent with the thermochemical properties of pre-carbonized structures. Herein, T_4, T_6, T_8, and T_{10} denote the pyrolysis temperatures as 400°C, 600°C, 800°C, and 1000°C respectively.

Proximate analysis shows a consistent decrease in VM with increasing pyrolysis temperature, reflecting enhanced devolatilization. FC correspondingly increases due to progressive carbon enrichment. Ash content generally increases or remains stable in NLB due to the concentration of inorganics, whereas HLB exhibits slightly lower ash content, likely attributed to mineral leaching during hydrothermal treatment [41].

3.2. Morphological and textural analysis of derived biochar

SEM analysis demonstrated significant morphological changes and distinct structural evolution in both NLB and HLB throughout the pyrolysis temperature range of 400–1000°C, as demonstrated in Fig. 2. The NLB samples exhibited a distinct fiber-bundle layout that progressively

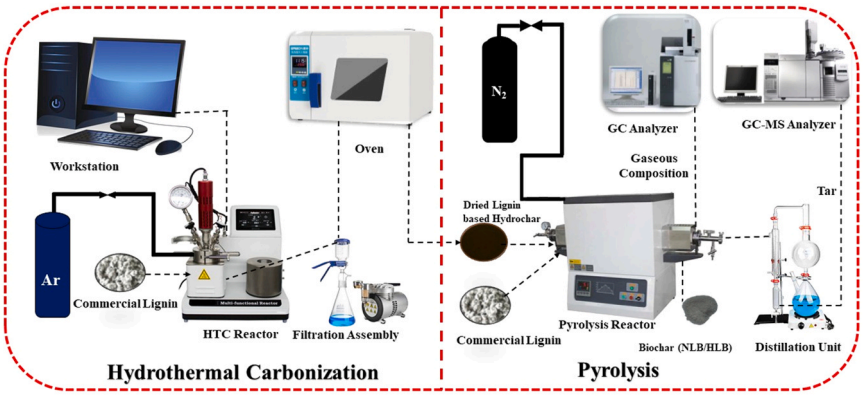

Fig. 1. Integrated HTC-Pyrolysis Experimental Setup.

Table 2
Ultimate and Proximate analysis of NLB and HLB during pyrolytic temperatures.

Samples	Ultimate Analysis (wt%)					Proximate Analysis (wt%)		
	C	H	N	S	O	Ash_d	FC_d	VM_d
NLB-T_4	37.33	2.06	0.78	0.04	23.78	36.00	33.00	31.00
NLB-T_6	38.20	1.79	0.72	0.06	18.99	40.24	38.50	21.26
NLB-T_8	39.82	1.24	0.70	0.06	7.04	51.13	32.79	16.08
NLB-T_{10}	40.15	0.99	0.64	0.06	4.31	53.84	32.68	13.48
HLB-T_4	37.00	1.90	0.65	0.05	20.79	39.60	30.44	29.96
HLB-T_6	36.23	1.84	0.71	0.05	26.71	34.45	37.63	27.92
HLB-T_8	33.60	1.72	0.76	0.05	32.87	31.00	45.00	24.00
HLB-T_{10}	29.42	1.35	0.60	0.05	38.58	30.00	48.00	22.00

d: dry basis.
$FC_d = 100\text{-}V_d\text{-}A_d$.
$O_d = 100\text{-}A_d\text{-}C_d\text{-}H_d\text{-}N_d\text{-}S_d$.

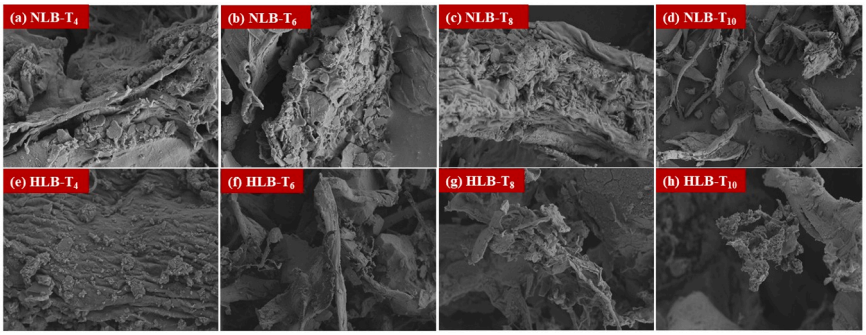

Fig. 2. Morphological structure of NLB (a-d), HLB (e-h).

transitioned into a tubular shape with the temperature rise. This morphological growth illustrates the inherent polymeric aromatic structure of LB, which preserves its structural integrity regardless of high temperatures. NLB samples exhibit uniform appearance at all temperatures (NLB-T_4 to NLB-T_{10}), indicating the untreated LB's established thermal decomposition pathway. On the other hand, HLB samples exhibited a morphological transformation. At lower temperatures (HLB-T_4), accumulations of particulate matter predominated over the biochar surface. With an increase in pyrolysis temperature, the initial framework transitioned into specified agglomerated structures, a characteristic that was completely lacking in NLB samples.

The HLB samples exhibit a heterogeneous, coarse surface morphology with a moderately porous structure. The particles predominantly appear as agglomerated fragments with irregular and non-agglomerated geometries, lacking smooth or uniform contours. This morphological pattern is consistent with the structural rearrangement and carbon densification processes typically induced during HTC, followed by thermal decomposition in pyrolysis, as illustrated in Fig. 2 (e–h). The unique morphological features (tubular for NLB and agglomerated rough structure for HLB) remained consistent across the whole temperature range, even though aromatization processes in pyrolysis transformed oligomers into aromatic hydrocarbons in both materials. This morphological determination proves that HTC pretreatment effectively changes the LB structural framework, yielding a distinct carbonaceous material, making this approach a suitable approach for controlled selectivity. This mechanism supports increased porosity and enhanced gas evolution under pyrolysis.

Pyrolysis-derived NLB samples exhibited a distinct non-monotonic evolution in their textural properties. Before dropping to 22.37 m^2/g (NLB-T_{10}), Table 3 showed the S_{BET} rising from 1.69 m^2/g (NLB-T_4) to 106.24 m^2/g (NLB-T_6) and 112.76 m^2/g (NLB-T_8). At the same time, the value of D_p shows a negative trend, falling between 14.77 nm and 2.45 nm (400–600°C), before rising to 18.84 nm (1000°C). This unusual trend matches SEM findings, suggesting that fiber-bundle shape moved into tubular forms before a structural collapse. Significant fragmentation of the NLB-T_6 structure at 600°C produced numerous micropores [42], thereby promoting a decrease in D_p even with a higher S_{BET}. The maximum porosity achieved at 800°C corresponds to thermal pyrolysis leading towards micropores formation, as also observed by Guo et. al (2006) [43]. For NLB-T_{10}, a dramatic drop in S_{BET} and a rise in D_p at 1000°C pyrolysis temperature was caused by the release of volatile matter, promoting pore collapse [44]. On the other hand, HLB showed a steady rise in S_{BET} (3.33–67.53 m^2/g) and V_p (0.015–0.1088 cm^3/g) between the applied temperature range (T_4 to T_{10}), as also evidenced from Zhu et. al (2015) [45]. Higher temperatures cause the enhanced structural stability and restructured carbon matrix, as evident through agglomerated morphology observed in SEM analysis, thereby promoting better results in pyrolytic performance, as also demonstrated in Figs. 7-8.

The non-monotonic BET trend in NLB samples reflects the natural pyrolytic behavior of LB, which is fundamentally changed through strategic HTC pretreatment. These findings support studies indicating that biomass pretreatment can significantly alter the qualities and thermal stability of biochar [46,47].

Table 3
Textural Properties of pyrolytic biochar derived from HTC-treated and non-treated LB.

Temperature	Samples	S_{BET} (m^2/g)	V_P (cm^3/g)	D_P (nm)
400°C	NLB-T_4	1.6873	0.006230	14.7682
	HLB-T_4	3.3304	0.015552	18.6783
600°C	NLB-T_6	106.2363↑	0.065106↑	2.4514↓
	HLB-T_6	19.9743↑	0.049296↑	13.8746↓
800°C	NLB-T_8	112.7647↑	0.139629↑	4.9529↑
	HLB-T_8	36.6182↑	0.083040↑	9.0709↓
1000°C	NLB-T_{10}	22.3670↓	0.1053345↓	18.8393↑
	HLB-T_{10}	67.5268↑	0.1088814↑	6.4457↓

3.3. Chemical functionality and structural framework analysis: crystalline order and carbon hybridization

The surface functional units of both pyrolytic biochar (NLB and HLB) were examined using FTIR analysis, as seen in Fig. 3. The FTIR spectra exhibit a broad absorption band centered around 3400 cm^{-1} , attributed to O–H stretching vibrations, confirming the presence of hydroxyl groups in both aliphatic and phenolic structures within lignin. A shoulder near 1700 cm^{-1} corresponds to C═O stretching of conjugated carbonyl groups, such as aldehydes and ketones, potentially originating from native lignin functionalities or mild oxidative reactions during HTC. The prominent bands at ~1600 and 1510 cm^{-1} are characteristic of aromatic skeletal vibrations, indicating the retention of lignin's aromatic backbone [48].

Absorptions near 2920 cm^{-1} and 2850 cm^{-1} are associated with C–H stretching in aliphatic –CH_3 and –CH_2 groups, reflecting the persistence of lignin side chains. The peak at ~1450 cm^{-1} further supports the presence of aliphatic C–H deformations. A distinct band at ~1260 cm^{-1} suggests guaiacyl-type lignin structures, indicative of ring breathing and C–O stretching typical of softwood-derived lignin. Weaker bands in the 1260–1220 cm^{-1} range suggest partial cleavage of aryl–ether linkages, corroborating depolymerization during HTC. Peaks within 1120–1020 cm^{-1} are linked to C–O stretching in aliphatic alcohols and ether bonds, supporting the presence of secondary alcohols. These spectral changes suggest that HTC encourages partial deoxygenation and structural condensation while maintaining the aromatic framework, an advantageous modification for subsequent thermochemical valorization.

In summary, comparing the results of FTIR analysis with pyrolysis indicates that the presence of numerous oxygen-containing functional groups (including methoxy, the hydroxyl group, carbonyl, carboxyl, etc.) contributes to the complexity of the LB structure, which in turn complicates the LB pyrolysis reaction. Oxygen-containing functional groups influence every stage of the reaction mechanism via electrons and steric factors; however, they do not impact the structure as well as geometry of precursors, transitional states, and intermediates. The type and quantity primarily influence pyrolysis rate, reactivity, and overall distribution of pyrolysis products.

Figs. 4a and 4b display the XRD patterns of NLB and HLB biochar at pyrolysis temperatures ranging from 400 to 1000°C, illustrating unique crystallographic trends that directly correspond with additional characterization findings. NLB samples (Fig. 4a) exhibit distinctive diffraction peaks at $2\theta \approx 26–27°$ and 29–30° corresponding to the carbon (002) peak [49]. As the temperature rises from 400°C to 600°C, the variations in peak intensity correspond with a significant increase in BET surface area (Table 2, from 1.69 to 106.24 m^2/g), thereby confirming that structural reorganization promotes micropore formation. At 800°C, additional peak development is associated with the highest surface area (112.76 m^2/g) and the smallest pore diameter (4.95 nm). At 1000°C, notable crystallographic reorganization accompanied by augmented diffuse scattering in the 20–30° range correlates with heightened D-band intensity in Raman spectra (Fig. 5a) and the collapse of the microporous structure, as indicated by a reduced surface area (22.37 m^2/g) and an increased pore diameter (18.84 nm).

HLB samples (Fig. 4b) exhibit markedly divergent behavior. At 400°C, the diffraction pattern reveals altered inorganic constituents and carbon structure, supported by FTIR results (Fig. 3) indicating heightened carbonyl content and partial aromatization. As the temperature increases, HLB demonstrates a regulated transformation: at 600–1000°C, stable crystalline characteristics correspond with a progressive rise in BET surface area (19.97–67.53 m^2/g) and a systematic reduction in pore diameter (13.87–6.45 nm). The XRD results are in strong agreement with the Raman spectroscopy findings (Fig. 5a, b), as both methods validate the elevated defect concentration in HLB samples. The elevated I_o/I_1 ratio in HLB Raman spectra corresponds to the maintained crystalline structure in XRD patterns, signifying improved thermal stability. XPS analysis (Fig. 6) corroborates these observations by indicating binding energy shifts that signify structural alterations. This finding demonstrates that HTC pretreatment fundamentally modifies the structural evolution of LB during pyrolysis, resulting in an optimized selectivity with synergistic interactions between carbon structure and inorganic components. The improved thermal resilience directly enhances syngas production efficiency as explained in Section 3.5.1, resulting in elevated H_2 yields and diminished CO_2 emissions.

Fig. 5 illustrates the Raman spectra of NLB and HTC at pyrolysis temperatures ranging from 400 to 1000°C, revealing carbon hybridization states consistent with other characterization results. The samples exhibit clear D-band (~1350 cm^{-1}) and G-band (~1580 cm^{-1}) characteristics, which suggest the presence of defect-induced vibrations in sp^2 carbon rings as well as in-plane stretching of sp^2 carbon bonds [50]. With an increase in pyrolysis temperature, both bands exhibit greater definition, and the D-to-G intensity ratio (I_o/I_1) increases in both samples. The evolution of the I_o/I_1 ratio in NLB samples (Fig. 5a) corresponds with the non-monotonic textural properties observed in the BET analysis (Table 3). The increase in defect concentration results in the formation of micropores, which significantly elevates the surface area from 1.69 to 112.76 m^2/g within the temperature range of 400–800°C. The wider D-band features observed at 1000°C suggest the presence of larger, disordered graphitic domains.

This phenomenon is associated with a decrease in surface area, measured at 22.37 m^2/g, and an increase in pore diameter, recorded at 18.84 nm. HLB samples (Fig. 5b) exhibit broader D-bands and a reduced number of valleys between the D and G bands compared to NLB, suggesting the presence of structural disorder. The FTIR results (Fig. 3)

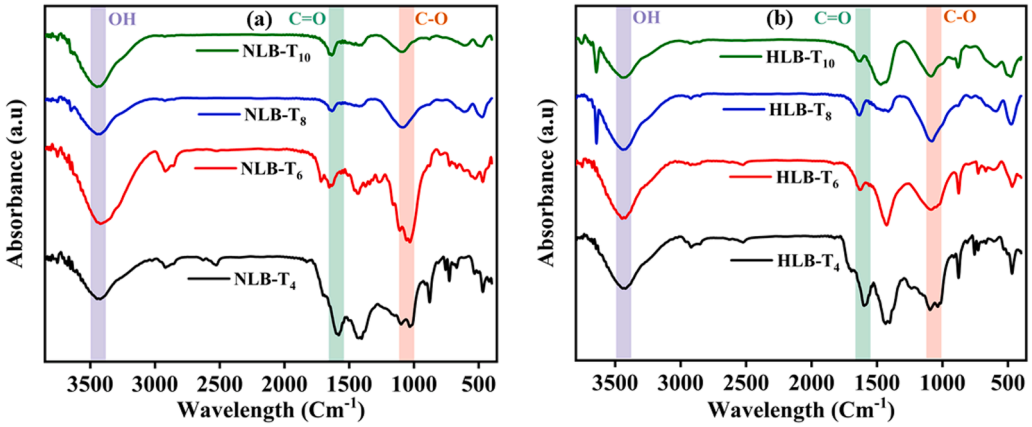

Fig. 3. FTIR spectrum of **(a)** NLB (T_4-T_{10}), and **(b)** HLB (T_4-T_{10}).

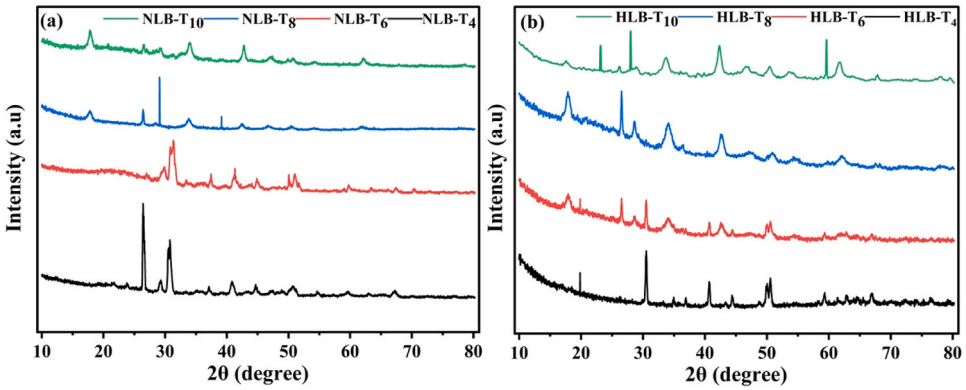

Fig. 4. XRD spectrum of **(a)** NLB (T_4-T_{10}), and **(b)** HLB (T_4-T_{10}).

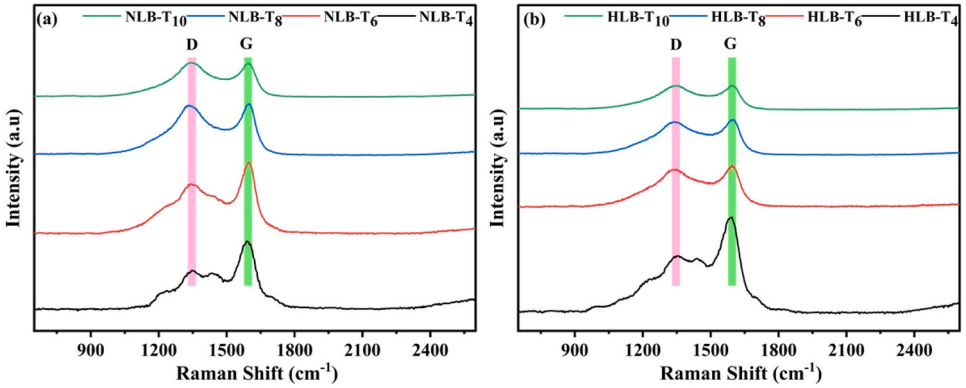

Fig. 5. Raman spectrum of **(a)** NLB (T_4-T_{10}), and **(b)** HLB (T_4-T_{10}).

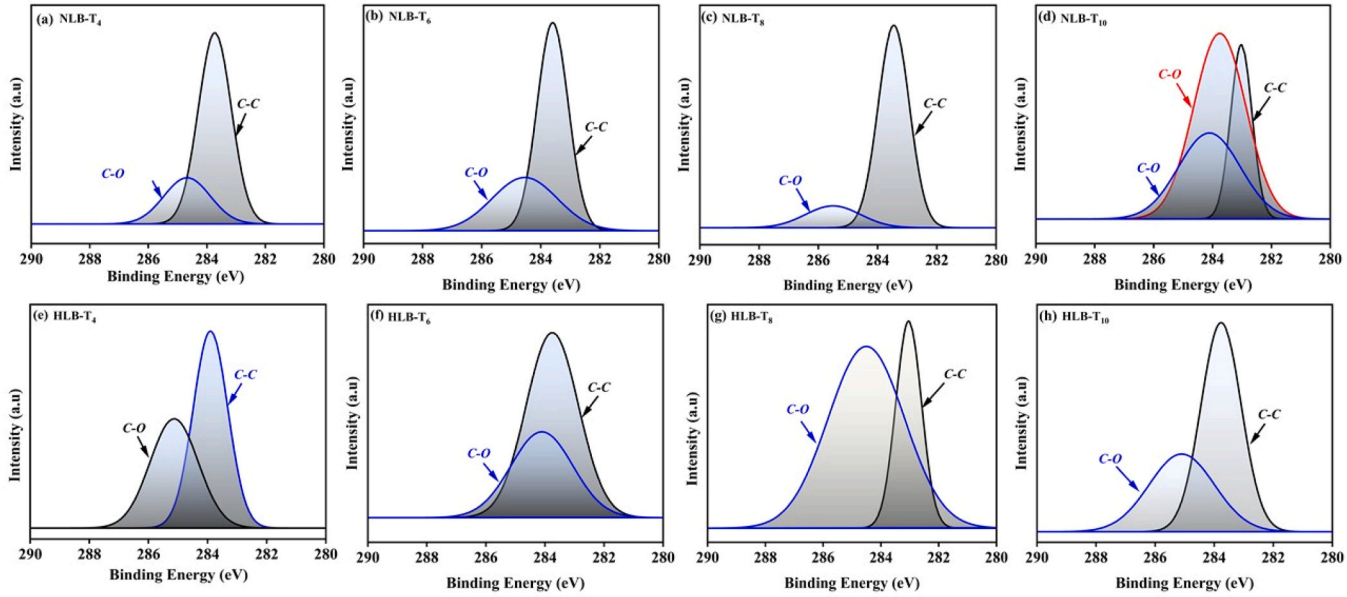

Fig. 6. XPS Spectra of NLB (a-d), and HLB (e-h).

indicate a rise in carbonyl content and a degree of aromatization following HTC pretreatment. Defect-rich carbon structures facilitate the development of controlled porosity by enhancing the BET surface area from 3.33 to 67.53 m^2/g and reducing the pore diameter from 18.68 to 6.45 nm within the specified temperature range. Refer to Figs. 4a and 4b. The XRD patterns validate the observations, showing diffuse scattering within the 20–30° 2θ range, which corresponds with the defect-rich carbon structures identified through Raman spectroscopy. XPS analysis, through the deconvolution of C1s spectra, verifies that the proportions of sp^2 and sp^3 carbon align with the Raman ID/IG ratios. This comprehensive examination reveals that HTC pretreatment results in a carbon structure abundant in defects, which endures high-

temperature conditions.

3.4. Surface chemistry analysis

Fig. 6 displays the C1s XPS spectra of both NLB and HLB biochars, highlighting the temperature-dependent variations in carbon chemical environments. At 400°C, Fig. 6a (NLB-T₄) shows a prominent C-C peak (~284.5 eV) alongside moderate C-O content (~286.0 eV). In contrast, Fig. 6e (HLB-T₄) reveals a marked increase in C-O intensity, indicating that HTC pretreatment enhances surface oxygen functionalities prior to pyrolysis. As the temperature rises to 600°C, Fig. 6b (NLB-T₆) demonstrates a decrease in C-O intensity, indicative of ongoing thermal decomposition. In contrast, Fig. 6f (HLB-T₆) exhibits a higher C-O/C-C ratio compared to NLB-T₆, suggesting enhanced retention of oxygen functionality, which aligns with the moderate BET surface area development of 19.97 m^2/g presented in Table 2. At 800°C, Fig. 6c (NLB-T₈) shows a further reduction in C-O content, indicating advanced deoxygenation. In contrast, Fig. 6g (HLB-T₈) maintains significant C-O functionality with a broader peak profile, suggesting the preservation of diverse carbon-oxygen bonding environments at elevated temperatures. The sustained oxygen functionality aligns with the increased defect concentration noted in the Raman spectra (Fig. 5b). At 1000°C, Fig. 6d (NLB-T₁₀) indicates the presence of a C═O component (~288.5 eV) with minimal C-O content, while Fig. 6h (HLB-T₁₀) shows substantial C-O functionality at this temperature, highlighting the remarkable thermal stability of oxygen groups in HTC-treated LB. This preserved functionality directly supports an increase in H_2 production capacity by 38 % through enhanced water-gas shift and reforming reactions. The temperature-specific XPS analysis demonstrates that HTC pretreatment significantly modifies the deoxygenation pathway of LB, with HLB samples preserving strategically distributed oxygen functionalities across the temperature spectrum, thereby fostering an optimal catalytic environment for improved syngas production efficiency. These oxygen-containing groups (e.g., carboxyl, phenolic, and carbonyl) act as catalytic sites by facilitating electron transfer and reactive radical formation, which promotes C–C and C–O bond cleavage during pyrolysis. This catalytic behavior enhances the conversion efficiency and syngas yield by lowering the energy barrier for gas-phase product evolution[51].

3.5. Pyrolysis characteristics

3.5.1. Effects of pyrolytic temperature on gaseous composition

The pyrolysis behavior of non-treated LB and HTC-treated LB reveals distinct temperature-dependent gas evolution patterns, driven by differences in chemical structure and oxygen functionality (Figs. 7a–b). Low- to moderate-temperature pyrolysis (≤300 °C) favors biochar retention, whereas higher temperatures (>300 °C) promote devolatilization toward syngas and condensable products.

For NLB, syngas comprises primarily H_2, CO, CO_2, and CH_4. Between 400–800 °C, H_2 decreases slightly (32.2 → 28.4 %) and CO from 33.8 → 25 %, indicating balanced dehydrogenation, decarboxylation, and decarbonylation rates. This stability suggests that most reactive oxygenated sites are consumed progressively, with minor secondary gas-phase losses. H_2 derives mainly from dehydrogenation of aromatic structures and heavy hydrocarbons, while CO forms via cleavage of C–O–C and C═O bonds, as supported by FTIR data. CH_4 and CO_2 rise moderately (5.4 → 6.4 % and 26.8 → 32.7 %, respectively), originating from methoxy (–OCH_3), methylene (–CH_2–), carbonyl, and carboxyl group breakdown [7,52]. NLB's lower oxygen removal during thermal processing results in higher CO_2 release. At 1000 °C, H_2 and CO decline sharply, likely due to gas-phase cracking, re-polymerization, and oxidation, underscoring the need for controlled temperature to preserve syngas quality. These findings underscore the temperature dependence of H_2 and CO, offering significant understanding into their behavior across different thermal conditions.

In contrast, HTC-treated LB exhibits a markedly different thermal behavior due to structural alterations induced by HTC pretreatment and alters the LB structure, enhancing its reactivity during pyrolysis [53]. H_2 and CO contents increase significantly with temperature (22.45 → 40.4 % and 32.3 → 33.4 %, respectively), reflecting enhanced thermal degradation of HTC-modified lignin. The cleavage of aromatic rings and oxygenated side chains in HLB promotes greater release of light gases, while intensified dehydrogenation liberates H_2 from both aliphatic and aromatic fragments. CO formation is favored through the breakdown of carbonyl and ether linkages, in agreement with FTIR analysis (Section 3.3). H_4 yield rises substantially (5.3 → 22.7 %), attributed to increased cracking of methoxy and methyl functionalities. Notably, CO_2 decreases sharply from 39.95 % to 11.5 %, as oxygen-rich carboxyl groups and inorganic carbonates are largely decomposed during HTC. Nevertheless, CO_2 production stops and its concentration falls after these carbonates are completely broken down [54].

The comparative trends confirm that HTC "pre-removes" oxygen primarily as CO_2 and H_2O (>90 % of HTC gas), reducing the O/C ratio and creating a more aromatic, carbon-rich matrix. This preconditioning redirects pyrolytic chemistry toward selective deoxygenation, boosting H_2 and CO yields while limiting CO_2. NLB, in contrast, retains more oxygenated moieties, leading to higher CO_2 evolution and lower overall syngas energy content.

In conclusion, HTC significantly improves syngas yield and quality while mitigating CO_2 release, positioning it as a promising pretreatment for optimizing LB pyrolysis. In addition to enhancing carbon retention and improving fuel properties, HTC facilitates the release of a minor fraction of gaseous products, predominantly carbon dioxide (CO_2, >90 %), generated primarily through decarboxylation and dehydration reactions under subcritical water conditions [55]. This initial evolution of CO_2 contributes to the subsequent reduction in CO_2 emissions observed during the pyrolysis of HTC-treated biomass, as a significant portion of thermally labile, oxygen-containing functional groups is

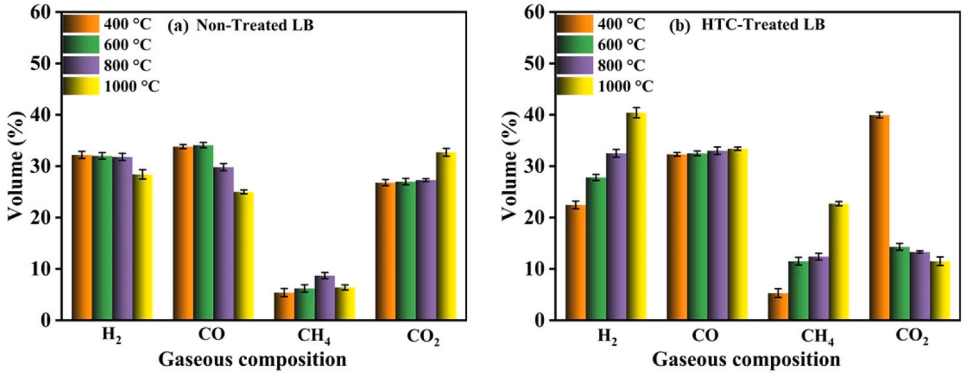

Fig. 7. Effects of different pyrolysis temperatures on the gaseous composition of non-treated LB and HTC.

removed during the HTC process. As a result, the chemical composition of the HC is altered, characterized by a lower O/C atomic ratio and a more aromatic, carbon-rich structure. These modifications suppress CO_2 formation during pyrolysis and promote enhanced syngas yield and quality due to improved thermal stability and devolatilization behavior. Overall, integrating the pyrolysis outcomes of both feedstocks demonstrate the clear advantages of HTC pretreatment: higher syngas yield, improved H_2/CO selectivity, and substantially reduced CO_2 emissions. These synergies position the HTC–pyrolysis cascade as a promising strategy for the efficient valorization of lignin-rich biomass into high-quality gaseous fuels.

3.5.2. *Effects of pyrolytic temperature on tar composition*

The composition of pyrolytic tar from non-treated LB and HTC-treated LB was analyzed based on standardized GC-MS peak area percentages, providing insights into temperature-dependent tar evolution. As illustrated in Fig. 8(a) and detailed in Table S-1, six major compound classes were identified in the liquid fraction: carboxylic acids, alcohols, furans, phenols, ketones, and polycyclic aromatic hydrocarbons (PAHs). The observed differences reflect the impact of HTC on LB structure and its subsequent pyrolytic pathways. In non-treated LB, carboxylic acids dominated across all temperatures, increasing steadily with temperature to a maximum of 28.08 % at 1000 °C. This trend arises from progressive thermal cleavage of lignin inter-unit linkages (β-O-4, α-O-4, C–C), producing intermediate aldehydes and phenolics that undergo further oxidation to acids under high-temperature cracking and rearrangement [56,57]. In contrast, phenolic compounds exhibited a steady decline with temperature. The potential explanation is that as the temperature increases, the bonds between the guaiacol units are not significantly disrupted, resulting in a lower formation of phenolic monomers [58]. This may be attributed to the thermal stability of guaiacyl-type structures in lignin, which resist depolymerization at elevated temperatures, thereby limiting the formation of free phenolic monomers. Furans, ketones, and esters occurred in minor proportions, with limited variation across the temperature range. At 1000 °C, the tar profile reflects the final decomposition stage of lignin, dominated by thermally stable acids and reduced phenolic content, indicative of extensive oxidation and secondary tar cracking.

In contrast, Fig. 8(b) illustrates the distribution of major organic compound categories in the tar from HTC-treated LB at varying pyrolysis temperatures. The predominant components follow the order: esters > carboxylic acids > phenols > furans ≈ ketones. The tar primarily consists of aromatic oxygenated compounds bearing functional groups such as –OH, –C═O, –COOH, and –C–O. Furan derivatives and additional organics, including acids, esters, alcohols, aldehydes, and aromatic hydrocarbons, were also detected (Table S-2). Key compounds with high relative abundance include 2-Dimethylaminomethyl-4-chloro-1-naphthol, isophthalic acid, and 1,4-benzenedicarboxylic acid methyl ester (Table S-2). Ester content increased with temperature, from 12.85 % to 27.48 %, peaking at 800 °C, then declined to 25.21 % at 1000 °C. This drop is likely due to thermal rearrangement forming phenolic derivatives, consistent with the literature [59]. At higher temperatures, phenols with alkyl groups become dominant due to cleavage of methoxy-bearing structures, such as guaiacol, and subsequent condensation. The generation of phenolic compounds is highly temperature-sensitive. Lower temperatures favor methoxyphenols, while higher temperatures promote alkylated phenols due to advanced fragmentation and conversion reactions. These outcomes underscore the structural transformation of LB under increasing thermal stress. Overall, the composition of tar varied irregularly with temperature. These fluctuations are attributed to: (I) the dynamic interplay of competing formation, cracking, and recombination reactions; (II) further decomposition of tar at high temperatures into lighter compounds; and (III) the presence of isomeric species with temperature-dependent behavior. Some tar may also adhere to biochar or reactor surfaces, especially at higher temperatures, affecting overall yield and composition. These findings highlight the complex thermal behavior of HTC-treated LB and provide mechanistic insight into optimizing tar quality through temperature control during pyrolysis. Mechanistically, HTC-treated LB tar evolution aligns with primary tar formation below 500 °C, followed by secondary and tertiary tar development at elevated temperatures. HTC-treated LB, however, enters pyrolysis with partially pre-cracked and deoxygenated structures, favoring ester formation at intermediate temperatures and phenolic enrichment under severe thermal stress. This enhanced reactivity allows for greater compositional tailoring via temperature control, offering pathways to optimize liquid product quality in HTC–pyrolysis cascades.

3.6. *Product distribution of HTC-pyrolysis cascade*

During HTC, LB is converted into solid HC and a liquid fraction. From 50 g of LB, 28.68 g HC (57.36 % yield) and 39.91 mL process water were obtained. The high solid yield reflects LB's aromatic, degradation-resistant structure, while the process water contains residual reaction water and dissolved organics from partial breakdown. Mass balance analysis revealed a pronounced temperature-dependent distribution of products during non-treated LB pyrolysis over 400–1000 °C under N_2. With increasing pyrolysis temperature from 400 to 1000 °C, char yield decreased from 70.0 to 56.0 wt%, gas yield increased from 18.5 to 38.0 wt%, and tar yield declined from 11.5 to 6.0 wt% as demonstrated in Fig. 9-a. The observed 14 wt% reduction in char and 5.5 wt% decrease in tar correspond to a 19.5 wt% increase in permanent gases, driven by enhanced devolatilization and secondary cracking of condensable volatiles at elevated temperatures. These trends are fully consistent with established slow-pyrolysis behavior, wherein elevated final temperatures reduce char yield and enhance gas formation, with

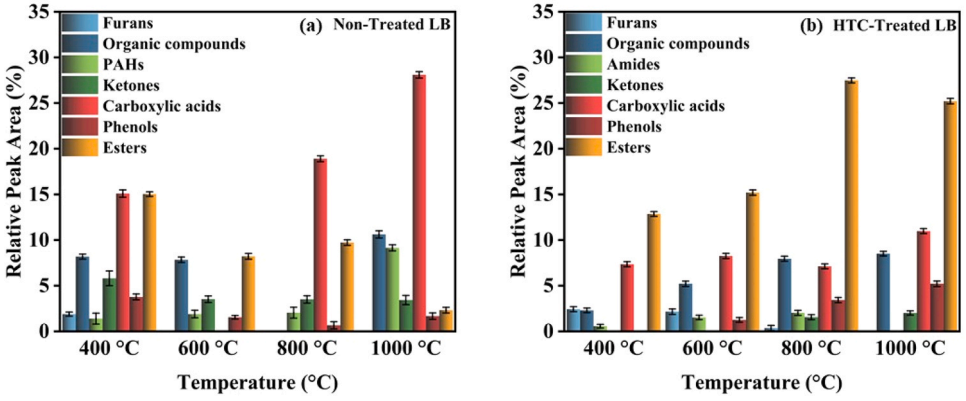

Fig. 8. Effects of different pyrolysis temperatures on the tar composition of non-HTC-treated LB.

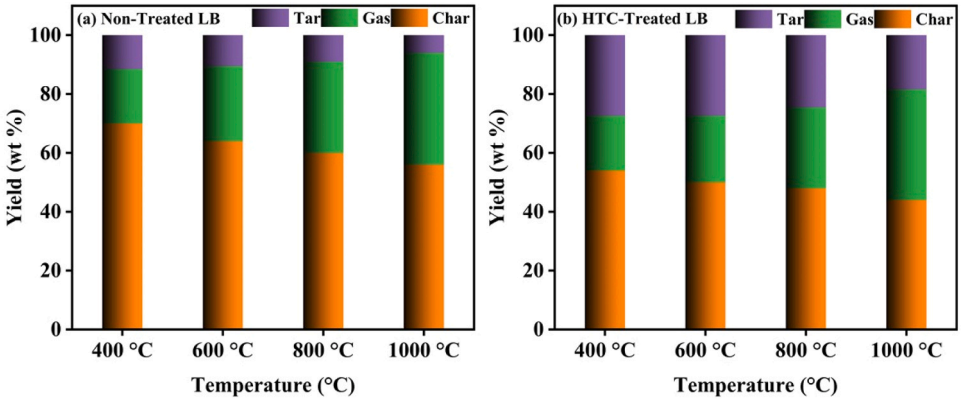

Fig. 9. Product distribution during pyrolysis of (a) Non-Treated LB, (b) HTC-Treated LB.

liquid production maximizing at intermediate temperatures (~500 °C) [60]. The comparatively high char retention observed here, particularly at higher temperatures, reflects lignin's broad decomposition range (200–900 °C) and its inherent char-forming propensity [61]. The close agreement between our measured mass balance and literature benchmarks strengthens the reliability of these findings and confirms that lignin-rich feedstocks consistently retain more solid carbon across the pyrolysis temperature spectrum. Gas Yield, Char yield, and Tar yield was calculated by following equations.

$$Gas\ yield(wt.\%) = \frac{m_{gas}}{m_{feed}} \times 100$$

$$Char\ Yield(wt.\%) = \frac{m_{char}}{m_{feed}} \times 100$$

$$Tar\ yield(wt.\%) = \frac{m_{tar}}{m_{feed}} \times 100$$

Char yield + Gas yield + Tar yield = 100%

For HTC-derived lignin biochar, with increasing the pyrolysis temperature from 400 to 1000 °C reduced char yield from 54.0 to 44.0 wt% and tar yield from 27.38 to 18.41 wt%, while gas yield increased markedly from 18.62 to 37.59 wt% as shown in Fig. 9-b. The 10 wt% decrease in char and 8.97 wt% decrease in tar correspond to a 18.97 wt % rise in permanent gases, indicating progressive devolatilization and enhanced secondary cracking of condensable volatiles at elevated temperatures. It promotes secondary char formation via tar repolymerization [42].

Tar yields in the mid-20 wt% range at moderate temperatures agree with the 20–30 wt% reported for lignin slow pyrolysis, and their decline at ≥ 800 °C reflects enhanced secondary cracking to gases. Gas yield

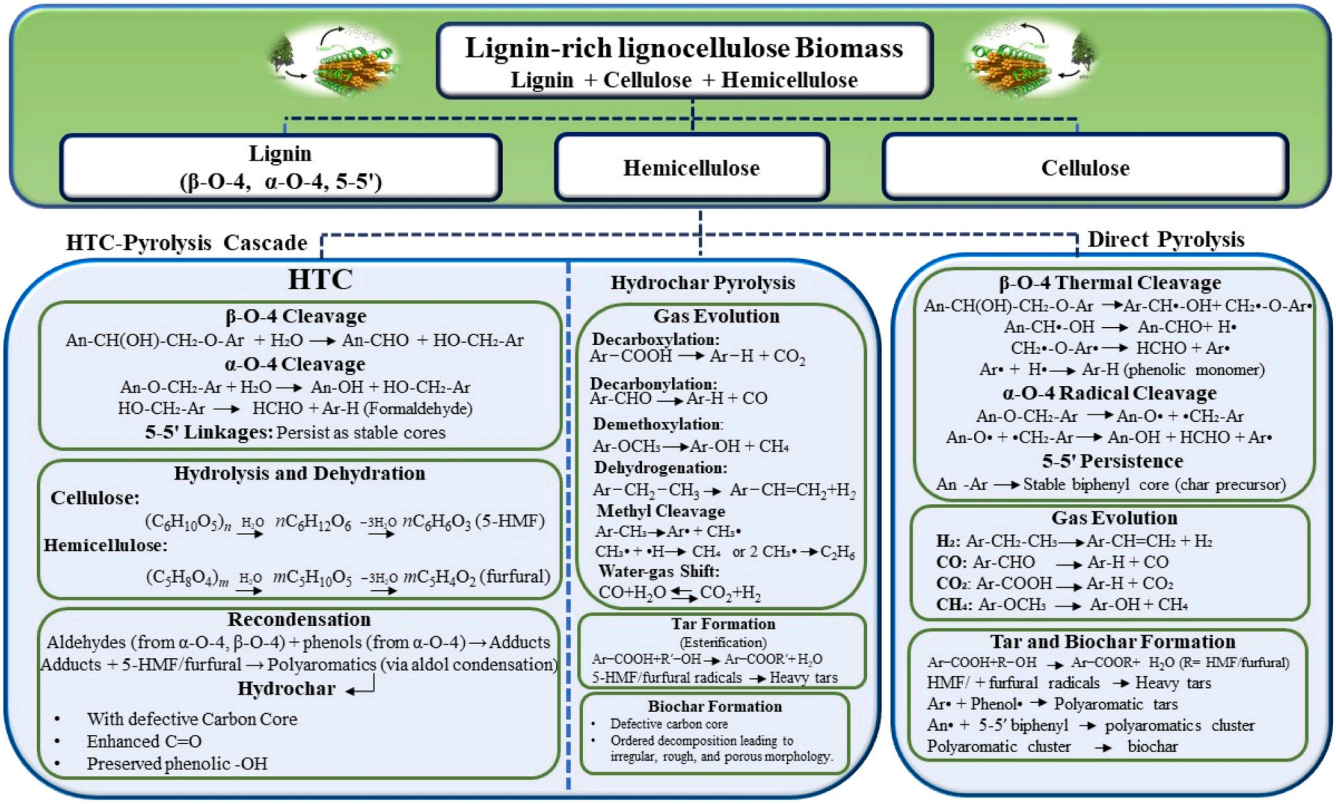

Fig. 10. Mechanism of integrated HTC-Pyrolysis.

trends inversely mirrored char and tar, increasing steadily with temperature as secondary reforming of vapors became dominant, consistent with literature showing greater CO, CO_2, CH_4, and H_2 production at higher severities [62]. Overall, the observed mass balance, high char retention, tar maximization at intermediate temperatures, and a monotonic gas increase, aligns strongly with established pyrolysis behavior for lignin-rich materials and validates the robustness of the experimental data.

3.7. Mechanistic insights into integrated HTC pyrolysis transformation pathways

HTC pretreatment profoundly changes the pyrolysis behavior of lignin-rich lignocellulosic biomass. Fig. 10 illustrates that HTC selectively cleaves major lignin linkages (β-O-4, α-O-4, 5–5′), depolymerizing and partially deoxygenating the biomass. The resulting HC has a lower O/C ratio and a more aromatic, cross-linked matrix than raw LB. Consequently, its pyrolytic decomposition follows modified pathways compared to direct pyrolysis. In untreated LB, lignin breaks down in stages: primary depolymerization (~400–500 °C) yields volatiles (e.g., guaiacols, syringols), then secondary cracking produces smaller aromatics and gases, and by ~800 °C tertiary reactions form polycyclic aromatic hydrocarbons (PAHs) and char. HTC-treated LB enters pyrolysis already "pre-cracked" and deoxygenated, allowing more efficient fragmentation with fewer secondary reactions needed. The thermal decomposition of biomass is governed by the reactivity of its carbonaceous components, which significantly influences the release of volatiles and the formation of solid products. Volpe et al., [63] proposed an innovative approach to quantify carbon reactivity by relating it to the elemental composition of process outputs, offering deeper insight into the mechanisms of biomass devolatilization. Incorporating such perspectives enhances our understanding of the thermal behavior of biomass and supports the interpretation of pyrolysis pathways in relation to feedstock chemistry. HTC pretreatment enhances selective bond cleavage and shifts deoxygenation toward H_2 and CO. Pyrolysis gases from HTC-treated LB contain significantly more H_2 and CO and much less CO_2 than gases from untreated biomass. This is because HTC removes reactive oxygen groups (as CO_2 and H_2O during the hydrothermal step), leaving fewer carboxyls to generate CO_2 in pyrolysis. Instead, remaining oxygen is often in carbonyl or ether form, which breaks to CO via decarbonylation.

The more aromatic HC also promotes dehydrogenation of its structure (cleavage of methoxy/methyl groups), leading to higher H_2 and CH_4 yields. The net result is that HTC–pyrolysis favors gas-phase reactions producing H_2 and CO, while suppressing decarboxylation reactions that release CO_2. Tar from HTC-treated LB pyrolysis is lighter and less polymerized than tar from direct pyrolysis. Untreated LB yields tar rich in heavy oxygenates (e.g., carboxylic acids) and, at higher temperatures, larger aromatic clusters as phenolic fragments recombine into PAHs. HTC-treated biomass produces tar dominated by smaller aromatic oxygenates (mono-phenols and esters) with very few multi-ring hydrocarbons. These tar intermediates are largely stabilized as single-ring compounds rather than condensing into heavy PAHs. Accordingly, the final char from HTC-treated LB is more graphitic (higher carbon order and surface area) and carries fewer tar residues than the char from raw LB pyrolysis.

4. Conclusion

This comprehensive approach of integrating HTC-Py for LB valorization yields new scientific understanding and performance improvements, thereby proving that LB pretreatment through HTC significantly restructures its physicochemical properties, making it an ideal feedstock for valuable pyrolytic products. Characterization via SEM, BET, FTIR, XRD, Raman, and XPS demonstrated increased aromaticity, optimized porosity, and controlled oxygen functionality in HTC-derived biochars (HLB). XRD and Raman spectra indicated semi-crystalline carbon with defect-rich domains, while XPS confirmed selective deoxygenation. These structural advancements promoted enhanced gas production and tar quality in HLB pyrolysis. Notably, syngas output improved markedly: H_2 yield reached 40.4 %, CO rose to 33.4 %, and CO_2 emissions dropped to 11.5 %. This reflects improved devolatilization and deoxygenation, enabling more efficient hydrogen and CO evolution. GC–MS analysis of tar revealed a favorable shift toward monoaromatic esters and phenolics without the need for catalytic support. These results underscore HTC's ability to reshape decomposition routes and enhance product selectivity. Overall, the HTC-pyrolysis cascade presents a catalyst-free, thermochemically optimized platform for generating H_2- and CO-rich syngas and valuable chemicals from LB. These findings support scalable biomass valorization strategies aligned with green energy and circular bioeconomy objectives. Tailored catalyst integration could further enhance H_2 and CO yields while reducing tar, supported by kinetic modeling and real-time pathway analysis. Co-pyrolysis with other feedstocks may balance reactivity and improve energy density, while techno-economic and life-cycle studies will guide scale-up. Investigating extractives and inorganics will enable predictive modeling and the design of efficient, low-emission conversion systems.

Author statement

We confirm that this manuscript is original and has not been published elsewhere, nor is it under consideration by any other publication. All authors have contributed significantly to the work, reviewed the final version of the manuscript, and approved its submission. We declare no conflict of interest. All reviewer and editor comments have been carefully addressed in this revised version. This research was conducted in compliance with relevant ethical standards.

CRediT authorship contribution statement

Xiaolong Zhou: Writing – review & editing, Visualization, Validation, Supervision, Resources, Project administration, Funding acquisition. **Muhammad Asif Nawaz:** Writing-review & editing, Validation, Co-supervision, and Funding acquisition. **Akash Kumar:** Writing – review & editing. **Asma Leghari:** Writing – review & editing. **Adil Mansoor:** Writing – review & editing. **Azhar Laghari:** Writing – review & editing. **Muhammad Rizwan:** Writing – review & editing, Writing – original draft, Visualization, Methodology, Investigation, Formal analysis, Data curation, Conceptualization.

Declaration of Competing Interest

The authors declare that they have no known competing financial interests or personal relationships that could have appeared to influence the work reported in this paper.

Acknowledgments

This research was sponsored by the Fundamental Research Funds for the Central Universities, along with the FLEXBY (GA-101144144), and (JDC2022-048533-I) Projects.

Appendix A. Supporting information

Supplementary data associated with this article can be found in the online version at doi:10.1016/j.jaap.2025.107342.

Data availability

Data will be made available on request.

References

[1] S. Kag, et al., Bioeconomy for sustainable bioenergy and biofuel generation. in Bioeconomy for Sustainability, Springer, 2024, pp. 83–105.
[2] X. Pan, et al., Toward efficient biofuel production: a review of online upgrading methods for biomass pyrolysis, Energy Fuels 38 (20) (2024) 19414–19441.
[3] J. Dong, et al., Effect of CaO addition on fast pyrolysis behavior of solid waste components using py GC/MS, J. Anal. Appl. Pyrolysis 188 (2025) 107055.
[4] S. Liu, et al., Comparable effects of manure and its biochar on reducing soil cr bioavailability and narrowing the rhizosphere extent of enzyme activities, Environ. Int. 134 (2020) 105277.
[5] G. Tian, et al., Efficient syngas conversion via catalytic shunt, Nat. Sustain. (2025) 1–12.
[6] X. Li, et al., Catalytic cracking of biomass tar for hydrogen-rich gas production: parameter optimization using response surface methodology combined with deterministic finite automaton, Renew. Energy 241 (2025) 122368.
[7] G. Li, et al., Regulating phenol tar in pyrolysis of lignocellulosic biomass: product characteristics and conversion mechanisms, Bioresour. Technol. 409 (2024) 131259.
[8] F. Sher, et al., Agglomeration behaviour of various biomass fuels under different air staging conditions in fluidised bed technology for renewable energy applications, Renew. Energy 227 (2024) 120479.
[9] H. Yang, et al., High-value utilization of agricultural waste: a study on the catalytic performance and deactivation characteristics of iron-nickel supported biochar-based catalysts in the catalytic cracking of toluene, Energy 323 (2025) 135806.
[10] V. Ashokkumar, et al., Advancements in lignocellulosic biomass: a critical appraisal of fourth-generation biofuels and value-added bioproduct, Fuel 365 (2024) 130751.
[11] D. Agrawal, et al., Novel approaches to alleviate lignocellulosic biomass waste for effective and sustainable utilization. in Value Addition and Utilization of Lignocellulosic Biomass: Through Novel Technological Interventions, Springer, 2025, pp. 89–116.
[12] Y. Xu, et al., Cooperative production of monophenolic chemicals and carbon adsorption materials from cascade pyrolysis of acid hydrolysis lignin, Bioresour. Technol. 399 (2024) 130557.
[13] A. Yousuf, D. Pirozzi, F. Sannino, Fundamentals of lignocellulosic biomass. in Lignocellulosic biomass to liquid biofuels, Elsevier, 2020, pp. 1–15.
[14] C. Vasile, M. Baican, Lignins as promising renewable biopolymers and bioactive compounds for high-performance materials, Polymers 15 (15) (2023) 3177.
[15] J.F. Rubio-Valle, et al., Valorization of lignin-rich solid residues from different eucalyptus wood conversion processes as oil structurants via electrospinning, Ind. Crops Prod. 222 (2024) 119442.
[16] Q. Zheng, et al., Unraveling the synergistic development of carbon skeleton and pore networks involved in lignin pyrolysis, J. Anal. Appl. Pyrolysis 170 (2023) 105912.
[17] K.L. Patle, et al., Nb2O5 supported metal-based heterogeneous catalysts for hydrodeoxygenation (HDO) of lignin-derived molecules: a powerful tool for generating fuel-additive products including hydrocarbons, Catal. Rev. (2025) 1–53.
[18] Q. Tian, et al., The driving force of biomass value-addition: selective catalytic depolymerization of lignin to high-value chemicals, J. Environ. Chem. Eng. 11 (3) (2023) 109719.
[19] N.I. Jeffri, et al., Unlocking the potential: evolving role of technical lignin in diverse applications and overcoming challenges, Int. J. Biol. Macromol. (2024) 133506.
[20] Z. Chen, C. Wan, Biological valorization strategies for converting lignin into fuels and chemicals, Renew. Sustain. Energy Rev. 73 (2017) 610–621.
[21] L.T. Nguyen, et al., Valorization of industrial lignin to value-added chemicals by chemical depolymerization and biological conversion, Ind. Crops Prod. 161 (2021) 113219.
[22] H. Durak, Comprehensive assessment of thermochemical processes for sustainable waste management and resource recovery, Processes 11 (7) (2023) 2092.
[23] A. Khosravi, et al., Production and characterization of hydrochars and their application in soil improvement and environmental remediation, Chem. Eng. J. 430 (2022) 133142.
[24] A. Picone, et al., Co-hydrothermal carbonization with process water recirculation as a valuable strategy to enhance hydrochar recovery with high energy efficiency, Waste Manag. 175 (2024) 101–109.
[25] M. Zhou, et al., Anaerobic digestion of process water from hydrothermal treatment processes: a review of inhibitors and detoxification approaches, Bioresour. Bioprocess. 11 (1) (2024) 47.
[26] A. Picone, et al., Role of reaction parameters in hydrothermal carbonization with process water recirculation: hydrochar recovery enhancement and energy balance, Biomass.. Bioenergy 181 (2024) 107061.
[27] K.G. Latham, et al., Impact of temperature and residence time on the hydrothermal carbonization of organosolv lignin, J. Anal. Appl. Pyrolysis 166 (2022) 105623.
[28] X. Zhuang, et al., Insights into the evolution of chemical structures in lignocellulose and non-lignocellulose biowastes during hydrothermal carbonization (HTC), Fuel 236 (2019) 960–974.
[29] U. Musa, et al., Effect of process variables on producing biocoals by hydrothermal carbonisation of pine kraft lignin at low temperatures, Fuel 325 (2022) 124784.
[30] A. Borrero-López, et al., Modelling the reactions of cellulose, hemicellulose and lignin submitted to hydrothermal treatment, Ind. Crops Prod. 124 (2018) 919–930.
[31] E. Atta-Obeng, et al., Physico-chemical characterization of carbons produced from technical lignin by sub-critical hydrothermal carbonization, Biomass. Bioenergy 107 (2017) 172–181.
[32] A. Kumar, et al., Assessing bioenergy prospects of algal biomass and yard waste using an integrated hydrothermal carbonization and pyrolysis (HTC–PY): a detailed emission–to–ash characterization via diverse hyphenated analytical techniques and modelling strategies, Chem. Eng. J. 492 (2024) 152335.
[33] A. Facchin, et al., Analytical evaluation of the coupling of hydrothermal carbonization and pyrolysis (HTC-Py) for the obtainment of bioavailable products, J. Anal. Appl. Pyrolysis 175 (2023) 106185.
[34] S.K. Hoekman, A. Broch, C. Robbins, Hydrothermal carbonization (HTC) of lignocellulosic biomass, Energy Fuels 25 (4) (2011) 1802–1810.
[35] A. Chauhan, et al., Oxidative cleavage of α-O-4, β-O-4, and 4-O-5 linkages in lignin model compounds over P, n Co-Doped carbon catalyst: a Metal-Free approach, ChemSusChem 17 (21) (2024) e202401049.
[36] M.-K. Bahng, et al., Current technologies for analysis of biomass thermochemical processing: a review, Anal. Chim. Acta 651 (2) (2009) 117–138.
[37] H. Guo, et al., Valorization of lignin to simple phenolic compounds over tungsten carbide: impact of lignin structure, ChemSusChem 10 (3) (2017) 523–532.
[38] J. Liang, et al., Interaction of derivatives of cellulose and lignin in co-HTC, co-pyrolysis and co-activation, Fuel 351 (2023) 129033.
[39] M. Yao, et al., Recent advances in lignin-based carbon materials and their applications: a review, Int. J. Biol. Macromol. 223 (2022) 980–1014.
[40] A. Leghari, et al., Influence of hydrothermal carbonized sewage sludge on coal water slurry performance, Front. Chem. Sci. Eng. 19 (1) (2025) 1–14.
[41] L. Chen, et al., Impact of low-temperature pyrolysis on ash and physicochemical properties of straw biochar: multivariate analysis and implications for agricultural and environmental use, Ind. Crops Prod. 224 (2025) 120431.
[42] R.K. Sharma, et al., Characterization of chars from pyrolysis of lignin, Fuel 83 (11-12) (2004) 1469–1482.
[43] Y. Guo, D.A. Rockstraw, Physical and chemical properties of carbons synthesized from xylan, cellulose, and kraft lignin by H3PO4 activation, Carbon 44 (8) (2006) 1464–1475.
[44] W. Ming-min, et al., Effect of pyrolysis conditions on the char surface area and pore distribution. Mei Ťan Hsueh Pao, Journal of China Coal Society, 2008, p. **33**.
[45] X. Zhu, et al., Investigation on the physical and chemical properties of hydrochar and its derived pyrolysis char for their potential application: influence of hydrothermal carbonization conditions, Energy Fuels 29 (8) (2015) 5222–5230.
[46] A. Ramos, E. Monteiro, A. Rouboa, Biomass pre-treatment techniques for the production of biofuels using thermal conversion methods–a review, Energy Convers. Manag. 270 (2022) 116271.
[47] H. Zhu, et al., The regulatory role of dissolved oxygen in N-doped biochar-driven nonradical oxidation, Chem. Eng. J. (2025) 165915.
[48] K.G. Tosin, N. Finimundi, M. Poletto, A systematic study of the structural properties of technical lignins, Polymers 17 (2) (2025) 214.
[49] S. Wang, et al., Influence of inherent hierarchical porous char with alkali and alkaline earth metallic species on lignin pyrolysis, Bioresour. Technol. 268 (2018) 323–331.
[50] C. Pardanaud, et al., Investigating the possible origin of Raman bands in defective sp2/sp3 carbons below 900 cm− 1: phonon density of states or double resonance mechanism at play? C 5 (4) (2019) 79.
[51] A.M. Robinson, J.E. Hensley, J.W. Medlin, Bifunctional catalysts for upgrading of biomass-derived oxygenates: a review, ACS Catal. 6 (8) (2016) 5026–5043.
[52] P. Kostetskyy, L.J. Broadbelt, Progress in modeling of biomass fast pyrolysis: a review, Energy Fuels 34 (12) (2020) 15195–15216.
[53] S. Inkoua, et al., Co-hydrothermal carbonization of fruit peel with sugars or furfural impacts structural evolution of hydrochar, Ind. Crops Prod. 193 (2023) 116221.
[54] D. Chen, et al., Insight into biomass pyrolysis mechanism based on cellulose, hemicellulose, and lignin: evolution of volatiles and kinetics, elucidation of reaction pathways, and characterization of gas, biochar and bio-oil, Combust. Flame 242 (2022) 112142.
[55] A. Funke, F. Ziegler, Hydrothermal carbonization of biomass: a summary and discussion of chemical mechanisms for process engineering, Biofuels Bioprod. Bioref. 4 (2) (2010) 160–177.
[56] J. Kang, S. Irmak, M. Wilkins, Conversion of lignin into renewable carboxylic acid compounds by advanced oxidation processes, Renew. Energy 135 (2019) 951–962.
[57] J. Yu, D. Wang, L. Sun, The pyrolysis of lignin: pathway and interaction studies, Fuel 290 (2021) 120078.
[58] J. Huang, et al., A computational study on thermal decomposition mechanism of β-1 linkage lignin dimer, Comput. Theor. Chem. 1054 (2015) 80–87.
[59] J. Li, et al., Slow pyrolysis experimental investigation of biomass tar formation and hydrogen production by tar reforming, Int. J. Hydrog. Energy 52 (2024) 74–87.
[60] M. del Carmen Recio-Ruiz, et al., An integrated approach to the valorization of pyrolysis products from lignocellulosic residues and by-products, Biomass. Bioenergy 196 (2025) 107676.
[61] M. Pahnila, et al., A review of pyrolysis technologies and the effect of process parameters on biocarbon properties, Energies 16 (19) (2023) 6936.
[62] A. Singh-Morgan, A. Puente-Urbina, J.A. van Bokhoven, Technology overview of fast pyrolysis of lignin: current state and potential for scale-up, ChemSusChem 15 (14) (2022) e202200343.
[63] R. Volpe, A. Messineo, M. Millan, Carbon reactivity in biomass thermal breakdown, Fuel 183 (2016) 139–144.